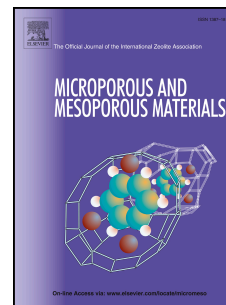


Journal Pre-proof

Preparation of mesoporous silica nanoparticles by spray drying

Lucía Gómez, Eva María Rivero-Buceta, Carla Vidaurre-Agut, Pablo Botella



PII: S1387-1811(25)00160-X

DOI: <https://doi.org/10.1016/j.micromeso.2025.113646>

Reference: MICMAT 113646

To appear in: *Microporous and Mesoporous Materials*

Received Date: 20 January 2025

Revised Date: 2 April 2025

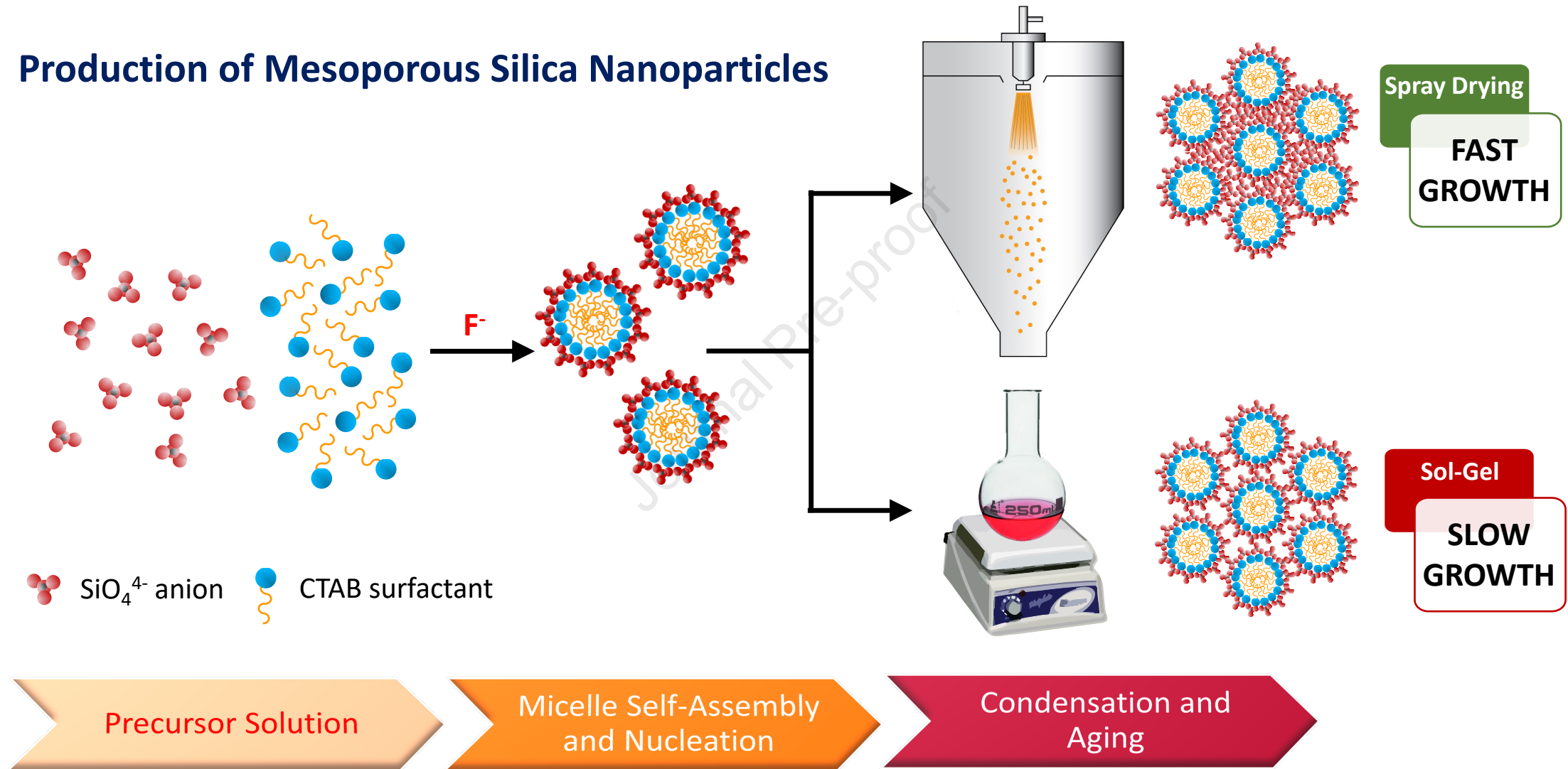
Accepted Date: 16 April 2025

Please cite this article as: L. Gómez, E.M. Rivero-Buceta, C. Vidaurre-Agut, P. Botella, Preparation of mesoporous silica nanoparticles by spray drying, *Microporous and Mesoporous Materials*, <https://doi.org/10.1016/j.micromeso.2025.113646>.

This is a PDF file of an article that has undergone enhancements after acceptance, such as the addition of a cover page and metadata, and formatting for readability, but it is not yet the definitive version of record. This version will undergo additional copyediting, typesetting and review before it is published in its final form, but we are providing this version to give early visibility of the article. Please note that, during the production process, errors may be discovered which could affect the content, and all legal disclaimers that apply to the journal pertain.

© 2025 Published by Elsevier Inc.

Production of Mesoporous Silica Nanoparticles



Preparation of mesoporous silica nanoparticles by spray drying

Lucía Gómez, Eva María Rivero-Buceta, Carla Vidaurre-Agut, Pablo Botella*

Instituto de Tecnología Química, Universitat Politècnica de València-Consejo Superior de Investigaciones Científicas, Avenida de los Naranjos s/n, 46022 Valencia, Spain

* To whom correspondence should be addressed. *E-mail:* pbotella@itq.upv.es. *Fax:* +34 96 3879444.

Journal Pre-proof

ABSTRACT

Mesoporous silica nanoparticles (MSNs) are usually obtained by conventional sol-gel synthesis techniques, in a process that requires long reaction periods, and goes through many critical steps. Small variation in the synthesis conditions can modify the morphology, structural and textural properties of materials. An alternative route for silica nanoparticles manufacturing is the spray drying (SD) technique, which involves particle formation by evaporation-induced hydrolysis and condensation of silicates, also providing continuous production. In this context, we have developed a new SD-based methodology for the preparation of well-dispersed MSNs by properly adjusting the pH of the synthesis mixture (e.g., pH=8.5), and using NaF as silica mobilizing agent. These nanoparticles present wormhole-like pores that are randomly distributed in all directions and hexagonal symmetry easily recognizable in the mesoporous wall at small domains. In addition, optimizing the gas inlet temperature (T_{in}) to 90°C promoted rapid assembly between silicate network building species during the SD process, yielding nanoparticles with good structural and textural properties. This technique is highly scalable and adaptable to the industrial stage, showing enormous interest in the pharmaceutical development.

Keywords:

Mesoporous silica nanoparticles; spray drying; fluoride media synthesis; Nano Spray Dryer; drug delivery.

1. Introduction

Mesoporous silica nanoparticles with MCM-41-type structure (MSNs) are characterized by large surface area and large pore volume, uniform and modulable pore size, easy surface functionalization (both internal and external) of the pores, and a rigid and stable hexagonal ordering [1]. MSNs are also very robust and present the ability to encapsulate metals and molecules within their pore channels [2,3]. These properties give MSNs potential applications in catalysis [4,5], separation [6], adsorption of chemicals [7] and biomedicine [8,9]. In the case of the biomedical scope, these MSNs can be utilized for the preparation of controlled drug delivery systems sensitive to chemical stimuli (pH, enzymes, redox compounds) or physical activation (temperature, light, magnetism and ultrasounds). MSN can also be used as multifunctional nanoplateforms encapsulating various contrast agents for subsequent diagnostic and imaging modalities, such as magnetic resonance imaging (MRI), optical/fluorescence, positron emission tomography (PET) and multimodality imaging [9,10]. In addition, these nanoparticles can effectively transport biomolecules such as nucleic acids and proteins conferring protection against enzymatic degradation [11]. However, the production of MSNs requires of conventional sol-gel synthesis techniques, in a process that takes long reaction periods, and goes through many critical steps (e.g., templating, nucleation, condensation, aging, separation, drying and template removal). Small variation in the synthesis conditions can condition the morphology, structural and textural properties of materials [12,13]. For example, the alkaline pH setting is critical, as lower initial pH results in amorphous nanoparticles, while a higher initial pH produces larger particles, and too high a pH often results in particle agglomeration [14]. In addition, reaction temperature and

surfactant concentration are other important parameters that influence the size and morphology of MSNs and are also known to alter the rate of hydrolysis and condensation rate of the silica precursor.

In this context, an alternative route recently developed for silica nanoparticles manufacturing is the spray drying (SD) technique [15]. This method involves particle formation through an evaporation-induced silicate hydrolysis and condensation. The process allows quick preparation of uniformly spherical silica particles in hydroalcoholic media from submicron to micron sizes, although different morphologies can be obtained by changing the solvent [16], and provides continuous production with strong potential for industrial scaling, which shows enormous interest in the pharmaceutical development [17]. Furthermore, currently, there is laboratory-scale equipment for the production of silica nanoparticles, as the Nano Spray Dryer B-90 introduced by BUCHI Labortechnik AG in 2009, which is able to produce spray-dried particles in the submicron scale with a narrow size distribution [18].

With regards to the preparation of mesoporous silica particles, some groups have succeed obtaining SBA-15 microspheres by SD with specific macroscopic properties [16,19], and also controlling the incorporation of drugs into the mesopores [16]. Nevertheless, the synthesis of MSNs by this method encounters several constrains, such as: i) the difficulties to assemble silicate anions and templating molecules in very short time leading to a partially structured material; ii) strong nanoparticle aggregation; and iii) technical limitations of the vibrating mesh spray technology, which can't be exposed to solutions of $\text{pH} > 8.5$. This last condition becomes critical because, as extensively studied by Varache et al. [20],

the optimal NaOH concentration for MSNs preparation is between 10 and 15 mM, with a pH set at 11.8.

It is possible to craft mesoporous molecular sieves by sol-gel condensation at almost neutral pH by using low molecular weight amines (e.g., ethanolamine) as silica activator [21]. Moreover, MCM-41 mesophase has also been synthesized with long-range structural order at low pH by using fluoride ions as mineralizing agent [22,23]. Therefore, we here present a new methodology based in SD for the preparation of well-dispersed MSNs with appropriate pH adjustment of the synthesis mixture (e.g., pH=8.5), and using different catalysts for silica activation, as NaOH, ethanolamine (ETA) or NaF. To our knowledge, this is the first successful attempt of synthesizing MSNs by the SD route starting from building components (e.g., silica source and templating agent), to give single nanoparticles with wormhole-like pores and hexagonal mesophase at small domains.

2. Experimental

2.1. Materials

Reagents and solvents were purchased from Sigma-Aldrich and used without further purification. Water was deionized to $18.2 \text{ m}\Omega \cdot \text{cm}^{-1}$ using a Milli-Q pack system.

2.2. Nano Spray Dryer B-90

The extensive description of the functional principle and operation are presented elsewhere [18]. Figure 1 presents schematically the operation for the production of MSNs.

Briefly, the liquid stream was atomized into fine droplets by a piezoelectric-driven vibrating mesh atomizer ($5.5 \text{ }\mu\text{m}$ droplet size), then subjected to drying in a drying chamber in order to yield solid particles and, finally, separated and collected by a suitable electrostatic dry powder collector. The standard working conditions were: pump at 60%

of maximum rate, 130 kHz vibration frequency, 35-45 mbar inlet pressure, 60% atomization rate, 125-135 L/min drying gas flow, 75-120 °C drying gas inlet temperature (T_{in}) and 40-50 °C gas outlet temperature. Spray drying operation was hold for 5 h, and afterwards the powder was gently collected from the internal wall of the electrode cylinder with a scraper.

2.3. Preparation of MSNs by Spray Drying

The initial solution was prepared in a 500 mL round bottom beaker with strong stirring at 25 °C. 0.50 g of hexadecyltrimethylammonium bromide (CTAB) was dissolved in 238 mL of a mixture water/ethanol 7:1 (v/v) (208 mL H₂O:30 mL EtOH). Subsequently, the corresponding mineralizer agent was added, NaOH, ETA or NaF. In all cases, pH was adjusted to 8.5 by adding, when needed, NaOH 0.1 M. After pH stabilization, 2.5 mL of tetraethylorthosilicate (TEOS) were dropped and the mixture was immediately pumped to the Nano Spray Dryer B-90.

For template removal, the collected powder at the Nano Spray Dryer B-90 was dispersed in 150 mL of HCl 0.25 M in ethanol and refluxed for 24 h. Afterwards, the suspension was filtered off and the extraction process repeated. Finally, the product was filtered off, washed with distilled water and freeze-dried at -55 °C. In the case of inorganic nanoparticles, removal of the water by a freeze-drying technique in a HyperCOOL Hyper-HC3110P-100 LabTech facility under optimized conditions resulted in MSN powders containing only weak secondary clusters [24,25], which could be easily redispersed in water or ethanol.

2.4. Preparation of MSNs in fluoride medium by the Sol-Gel process

0.50 g of hexadecyltrimethylammonium bromide (CTAB) was dissolved at 25 °C in 238 mL of a mixture water/ethanol 7:1 (v/v) (208 mL H₂O:30 mL EtOH) with strong stirring.

Subsequently, 118 mg of NaF were added and the pH was adjusted to 8.5 by adding NaOH 0.1 M. After pH stabilization, 2.5 mL of tetraethylorthosilicate (TEOS) were dropped and the mixture was stirred for 5 h. The initial gel composition (see also Table 1) was: 1:0.12:0.002:0.25:46:1036 SiO₂/CTAB/NaOH/NaF/EtOH/H₂O. Subsequently, the suspension was centrifuged (40 min, 33768 g), washed with distilled water and freeze-dried at -55 °C. The surfactant was removed in the same way that for samples produced by SD.

2.5. Materials characterization

XRD patterns were collected in a Philips X'Pert diffractometer equipped with a graphite monochromator, operating at 40 kV and 45 mA and using nickel-filtered Cu K α radiation $\lambda = 0.1542$ nm. Nitrogen gas adsorption isotherms were measured in a Micromeritics Flowsorb apparatus. Surface area calculations were carried out using the Brunauer–Emmett–Teller (BET) method, whereas pore size distribution was calculated according to the Kruk–Jaroniec–Sayari (KJS) estimation [26]. TEM micrographs were collected in a JEOL JEM 2100F microscope operating at 200 kV. When needed, particle diameter was calculated as the average with standard deviation of at least 250 measured nanoparticles. Samples for transmission electron microscopy (TEM) were ultrasonically dispersed in 2-propanol and transferred to carbon coated copper grids. Particle size and Z-Potential measurements were conducted by diffuse light scattering (DLS) in a Zetasizer Nano ZS (Malvern Instruments Ltd., Worcestershire, UK). Dried materials were re-suspended in deionized water at a concentration of 5 $\mu\text{g}/\text{mL}$ and measurements were performed at 25 °C. The mean hydrodynamic diameter was determined by cumulant analysis. Solid NMR spectra were recorded at room temperature under magic angle spinning (MAS) on a Bruker AV400 spectrometer. The single pulse ²⁹Si spectra were acquired using pulses of 3.5 μs corresponding to a flip angle of $3\pi/4$ rad and a recycle delay of 240 s. All spectra

were recorded with a 7 mm Bruker BL-7 probe and at sample spinning rate of 5 kHz, and referred to tetramethylsilane (TMS). The surfactant content in the as-synthesized materials was calculated from thermogravimetric analysis (TGA) in a Mettler-Toledo TGA/SDTA 851 e apparatus. Finally, the removal of surfactant after acid extraction was monitored by Fourier transform infrared (FTIR) and elemental analysis (EA). FTIR spectra were recorded at room temperature in the 400–4000 cm^{-1} region with a Nicolet 205xB spectrophotometer, equipped with a Data Station, at a spectral resolution of 1 cm^{-1} and accumulations of 128 scans. Elemental analysis was carried out in a FISONs, EA 1108 CHNS-O equipment.

3. Results

The initial gel compositions and yields of the as-synthesized samples are presented in Table 1. The physical-chemical properties of obtained mesoporous materials are described in Table 2.

Table 1. Compositional and structural characteristics of as-synthesized silica nanoparticles prepared by SD method and sol-gel synthesis.

Sample	Method	Temp. (°C)	Gel molar composition ^a							Y _{SiO₂} (wt%)	Y _{CTAB} ^b (wt%)	CTAB/SiO ₂ ^c (M)
			SiO ₂	CTAB	NaOH	EA	NaF	EtOH	H ₂ O			
SDN-1	SD	90	1	0.12	0.002	-	-	46	1036	15	85	1.20
SDN-2	SD	90	1	0.12	-	0.05	-	46	1036	49	74	0.32
SDN-3	SD	90	1	0.12	0.002	-	0.25	46	1036	44	94	0.45
SDN-4	SD	75	1	0.12	0.002	-	0.25	46	1036	41	72	0.37
SDN-5	SD	120	1	0.12	0.002	-	0.25	46	1036	41	90	0.46
SGN-1	Sol-Gel	25	1	0.12	0.002	-	0.25	46	1036	16	6	0.08

^a pH=8.5.

^b Calculated from TGA determination (loss of weight in the range 150-550 °C).

^c CTAB/SiO₂ ratio in spray-dried samples can be affected by CTAB accumulation on nanoparticle outer surface.

Table 2. Structural and textural characteristics of mesoporous silica nanoparticles prepared by SD method and Sol-Gel synthesis.

Sample	d_{hkl} -Spacing (Å)		S_{BET} (m ² g ⁻¹)	V_p (cm ³ g ⁻¹) ^a	D_p (Å) ^b	Sphere average diameter (nm) ^c	Pdl ^c	ζ -Potential (mV)
	d_{100}	d_{110}						
SDN-3	47.1	26.4	507.3	0.31	29.6	75.6 ± 32.4	0.184	-11.7
SDN-4	46.6	26.4	266.1	0.20	31.0	86.1 ± 40.9	0.226	-14.7
SDN-5	47.6	26.1	172.0	0.17	29.7	80.5 ± 38.4	0.228	-5.0
SGN-1	47.2	---	385.1	0.29	31.1	73.9 ± 32.4	0.193	-9.9

^a Adsorption cumulative volume of pores between 17.0 and 300.0 Å diameter.

^b As determined by the KJS estimation.

^c As determined by DLS.

3.1. Influence of the silica activator agent

We first tried to reproduce the sol-gel synthesis process in alkaline medium by SD in the Nano Spray Drier B-90. However, as commented before, the main technical limitation of this facility for MSNs production is the sensitivity to alkaline pH of the thin membrane in the piezoelectric-driven vibrating mesh atomizer (Figure 1, position 2), which quickly deteriorates for pH>8.5. This limits strongly the OH⁻ concentration in the initial synthesis gel, which makes compulsory using lower SiO₂/NaOH ratios (e.g., SiO₂/NaOH=0.002, see Table 1). Here, the formation of MSNs goes through four steps [27]: silica templating, nucleation, particle growth and surface aging. At almost neutral pH the hydrolysis of TEOS is slow [20] and the silica-surfactant micelles formation is minimized. Only when most of the solvent has been removed from the descendent droplets silica starts to condensate effectively. Thus, it is not surprising that when we carried out the SD of the synthesis mixture at standard working conditions and T_{in}=90 °C (SDN-1 sample) we obtained amorphous silica nanoparticles (average diameter 275.0 ± 66.5 nm, as determined by TEM), as the powder XRD file (Fig. 2a) and the TEM images (Fig. 3a) suggest.

As we needed to polymerize silica at mild alkaline pH, we tried to use an organic amine to accelerate the process. For instance, it has been reported that ETA acts as catalyst to mobilize and self-assemble the silica and the templating agent to produce microporous and mesoporous structures at neutral pH [21]. For the SD production, we adjusted pH=8.5 in the synthesis mixture with ETA (SDN-2, SiO₂/ETA=0.05, Table 1) and set T_{in}=90 °C but, unfortunately, we again obtained nanoparticles of amorphous silica (average diameter 71.8 ± 24.3, as determined by TEM), as it is reflected by the powder XRD pattern (Fig. 2b) and the TEM images (Fig. 3b and 3c).

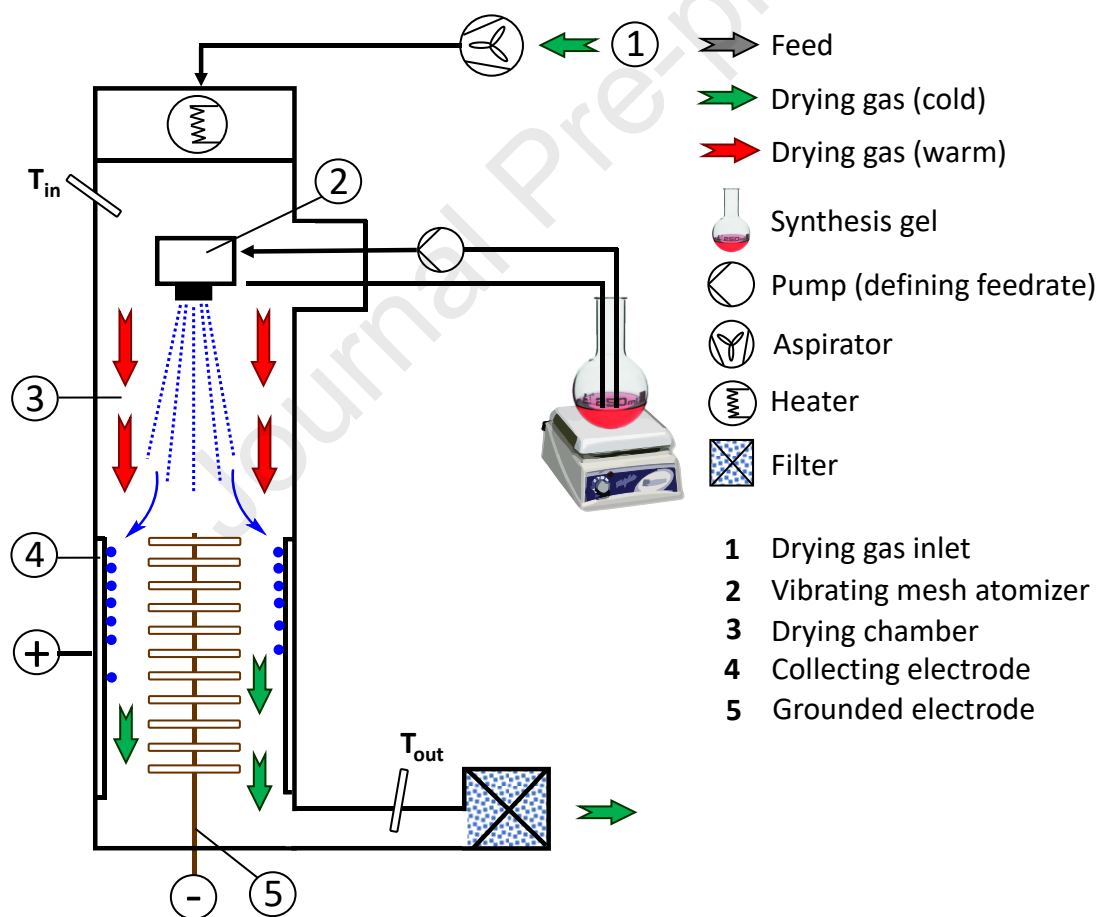


Fig. 1. Scheme of functioning and main components of the Nano Spray Dryer B-90 equipment.

At this point, F^- ion has been claimed to be a mineralizer that can replace successfully OH^- , due to the equivalent size and electronegativity of both anions [23]. Furthermore, fluoride group is able to mobilize and self-assemble silica with the structure directing agent (SDA) at neutral pH, and also stabilizes silicate network, by reducing the number of terminal hydroxyl groups (e.g., structural defects) on surface. Then, when we carried out the SD of the initial mixture (pH=8.5) at $T_{in}=90\text{ }^\circ\text{C}$ we obtained MSNs with hexagonal $P6mm$ ordering (sample SDN-3). The powder XRD pattern showed at least two discernible peaks indexed to (100) and (110) planes (Fig. 2c, Table 2).

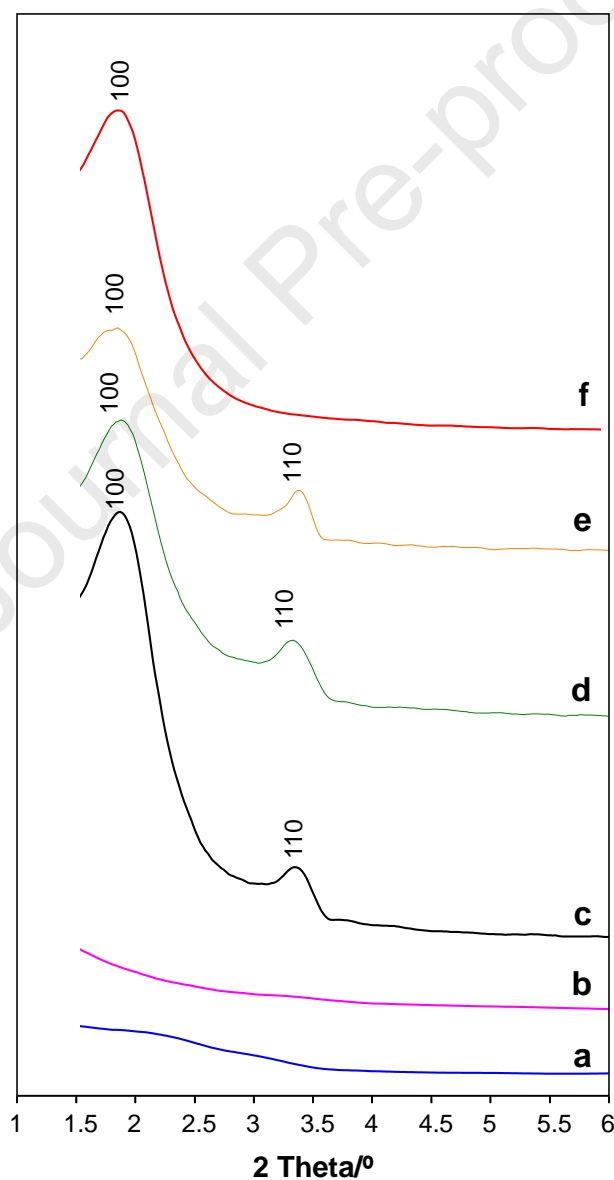


Fig. 2. Powder XRD patterns of as-synthesized materials: (a) SDN-1; (b) SDN-2; (c) SDN-3; (d) SDN-4; € SDN-5; (f) SGN-1.

Also, TEM (Fig. 3c) showed well-dispersed MSNs with a polydispersity index (PDI) of 0.184 and an average particle diameter of 75.6 ± 32.4 nm (as determined by DLS, see Table 2 and Fig. S1). SDN-3 sample showed a rather complex pore structure, in which the mesochannels were not ordered throughout the nanoparticle, but formed wormhole-like pores randomly distributed in all directions, starting at the center of the sphere and exiting towards the outer edge (Fig. 3e). However, the hexagonal symmetry was clearly visible when observing small domains of the mesoporous wall (inset of Fig. 3e).

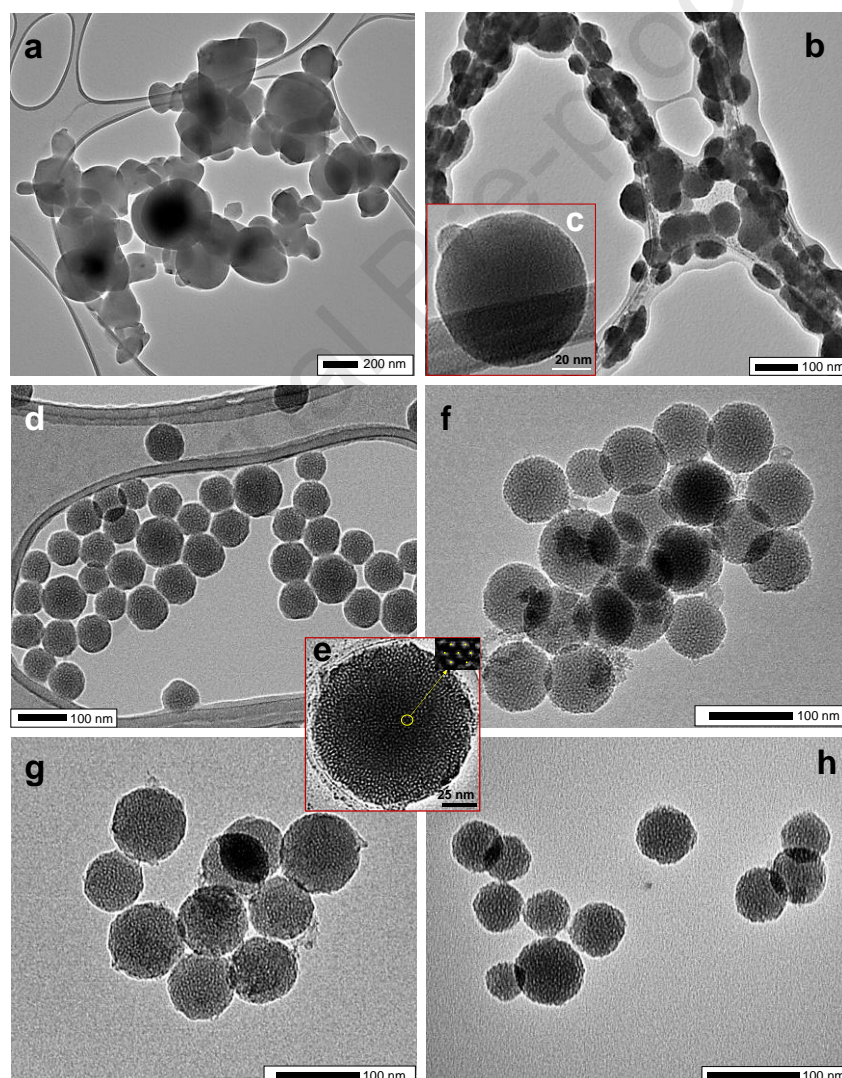


Fig. 3. Representative TEM images of the as-synthesized nanoparticles prepared by SD (a-e) or sol-gel (f) methods. (a) SDN-1; (b) SDN-2; (c) Detail of a nanoparticle of SDN-2 material showing no internal structure. (d) SDN-3; (e) Detail of a nanoparticle of SDN-3 material showing the internal structure formed by wormhole-shaped pores randomly

distributed in all directions. The inset shows the local arrangement in hexagonal $P6mm$ symmetry. (f) SDN-4; (g) SDN-5; (h) SGN-1.

The hexagonal ordering of this material was consistent with the obtained nitrogen adsorption report (Fig. 4a, Table 2), corresponding to a type IV isotherm (BET surface area, $S_{BET}=507.3 \text{ m}^2 \text{ g}^{-1}$) with narrow pore size distribution (pore diameter, $D_p=29.6 \text{ \AA}$, Fig. 4b, Table 2) and a relatively low pore volume ($V_p=0.31 \text{ cm}^3 \text{ g}^{-1}$) due to the imperfect hexagonal symmetry.

3.2. Influence of Spray Drying gas temperature

The most critical parameters to control during the SD process of MSNs are the templating compound, the silica precursor, the water content, the solvent and the temperature [28]. In this work, we used a standard synthesis gel composition in order to study the effect of the SD gas temperature on nanoparticles properties. Therefore, the inlet temperature of the airflow (T_{in}) was set at 75°C, 90 °C and 120 °C (respectively, SDN-4, SDN-3 and SDN-5 samples, Table 1), which determines the loss of solvent per unit of time and influences the structural and textural properties of the material. XRD patterns in Fig. 2 indicate that the mesoporous structure is already developed at $T_{in}=75 \text{ °C}$ (SDN-4 sample), although for $T_{in}=120 \text{ °C}$ (SDN-5 sample) the intensity of secondary reflection (110) is lowered. TEM images in Fig. 3 does not show any morphological difference among these samples, and no appreciable change in particle diameter was observed by DLS (Fig. S1). All samples presented type IV nitrogen adsorption isotherms (Fig. 4a), although S_{BET} changed significantly when increasing the drying gas temperature, with a maximum for the sample dried at $T_{in}=90 \text{ °C}$ (see Fig. 4c and Table 2). Here, the structure seems to collapse partially in SDN-5 sample, with a dramatic loss of surface area and pore volume (V_p). This external surface reduction with temperature was also consistent with the changes observed in Z-Potential, whose evolution maintained the same trend (Table 2).

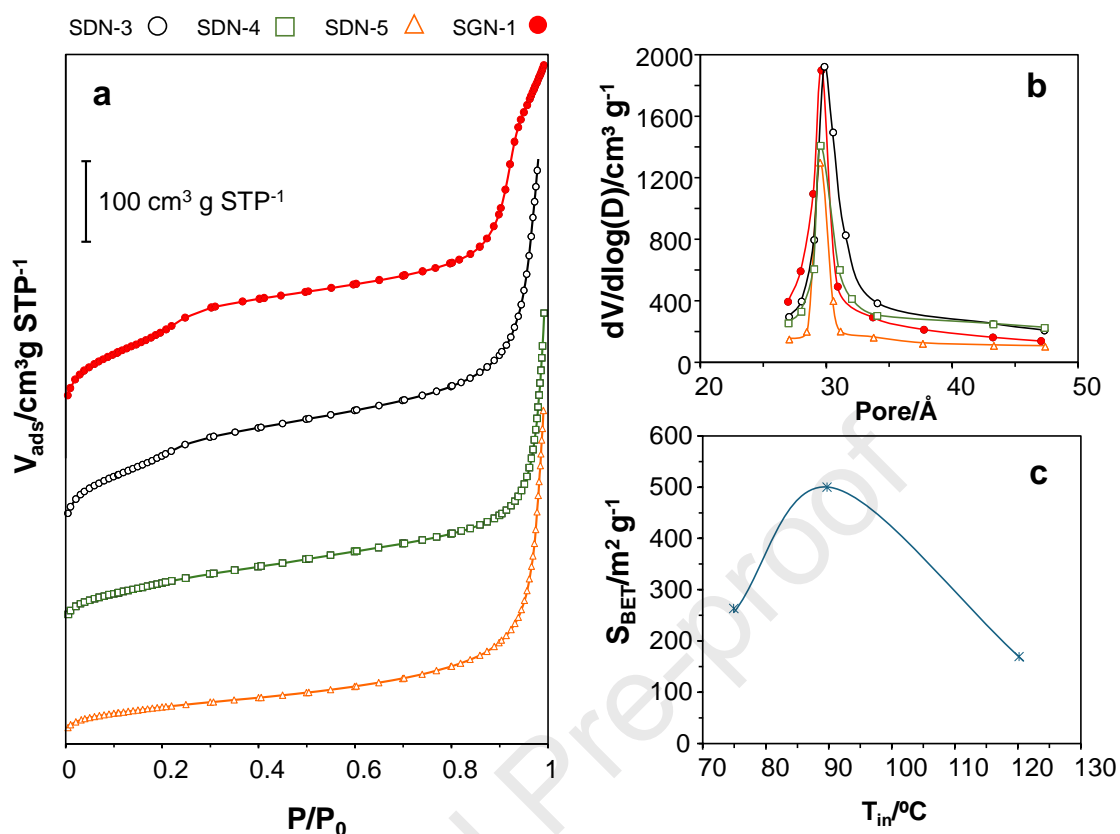


Fig. 4. Nitrogen adsorption isotherms (a), pore size distribution (b), and evolution of S_{BET} with T_{in} (c) of materials obtained by the SD method (SDN-3, SDN-4, SDN-5) or by sol-gel synthesis (SGN-1).

FTIR spectra indicated that after twice HCl-ethanol washing all samples showed only residual quantities of surfactant (Fig. S3). Two weak absorption peaks were detected $2924 cm^{-1}$ and $2852 cm^{-1}$ corresponding, respectively, to the asymmetric stretching vibration and symmetric stretching vibration for C-H on methylene groups [29,30]. Elemental analysis confirmed the removal of the template in MSNs, reporting less than 1% Carbon in all samples. In addition, FTIR study also provided information on the external silanols (Si-OH), with bands centered at $3452 cm^{-1}$ and $1650 cm^{-1}$ corresponding, respectively, to the stretching vibration and bending vibration of -OH groups [30].

3.3. Preparation of MSNs by Spray Drying versus Sol-Gel synthesis

For the purpose of comparison, we prepared MSNs in fluoride medium by the classical sol-gel process. The composition of the synthesis gel, the reaction temperature ($T=25\text{ }^{\circ}\text{C}$), and the reaction time ($t=5\text{ h}$) were the same that for the mixture fed to the Nano Spray Drier. The results showed, firstly, that the silica yield of the process was very low ($Y_{\text{SiO}_2}=16\%$, Table 1), which was due to the slow kinetic of the surfactant-silica interaction at $\text{pH}=8.5$, and the short time given to the starting components to react. After template extraction, the powder XRD pattern (Fig. 2f) corresponded to a disordered hexagonal wormhole-like structure, with a single diffraction peak indexed to (100), whereas no secondary reflections were detected (Table 2). This is in agreement with the observed morphology by TEM (Fig. 3f). Therefore, it is not surprising that SGN-1 material presented lower S_{BET} than SGN-3, due to the incomplete development of the hexagonal mesophase.

The ^{29}Si MAS NMR spectra (Fig. 5) of SDN-3 and SGN-1 showed high condensation level of silicate species in both samples, as expected from the used synthesis conditions. It has been reported that fluoride anion replaces hydroxyls in the silicate network, increasing the level of connectivity of silica in the lattice and reducing the percentage of structural defects, which results in a chemically more inert surface [23]. As a consequence, the quantity of Q_2 ($(\text{SiO})_2\text{Si}(\text{OH})_2$) and Q_3 ($(\text{SiO})_3\text{Si}(\text{OH})$) silicon environments is clearly dropped in as-synthesized materials. Therefore, deconvolution of the NMR signal in sample SGN-1 led to 4% of Q_2 ($(\text{SiO})_2\text{Si}(\text{OH})_2$ at -92.5 ppm), 31% of Q_3 ($(\text{SiO})_3\text{Si}(\text{OH})$ at -102.4 ppm), and 64% of Q_4 ($(\text{SiO})_4\text{Si}$ at -111.2 ppm). In the same way, SDN-3 material showed similar silica polymerization grade with 5% of Q_2 ($(\text{SiO})_2\text{Si}(\text{OH})_2$ at -92.3 ppm), 30% of Q_3 ($(\text{SiO})_3\text{Si}(\text{OH})$ at -102.6 ppm), and 65% of Q_4 ($(\text{SiO})_4\text{Si}$ at -111.3 ppm).

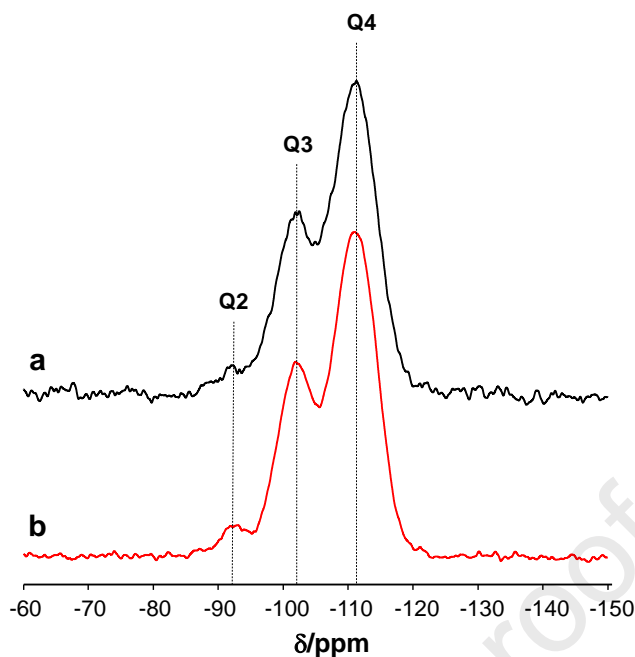


Fig. 5. Representative ^{29}Si MAS NMR spectra of as-prepared materials obtained by SD synthesis (a, SDN-3), or sol-gel process (b, SGN-1).

4. Discussion

As commented before, the formation of MSNs goes through four steps: templating, nucleation, condensation and aging. Templating and nucleation take place very quickly (a few minutes) [12], and it can be assumed that they are happening mostly at the liquid medium before the SD process starts. However, condensation and aging need of a larger period (6-48 hours), specially at neutral pH and room temperature. For spray-dried samples, these steps are accelerated by the fast drying at the hot airflow. The solvent elimination occurs in a few seconds, and the growth of the mesophase depends of an equilibrium between silicate anions condensation and water removal (Fig. 6). Unfortunately, for weak silica mobilizers like low alkali concentration or ETA, water removal happens too quickly to assure the right deposition of silicate units on the surface of CTAB micelles. In these conditions, most of the surfactant and SiO_4^{4-} anions condensate freely to give amorphous silica.

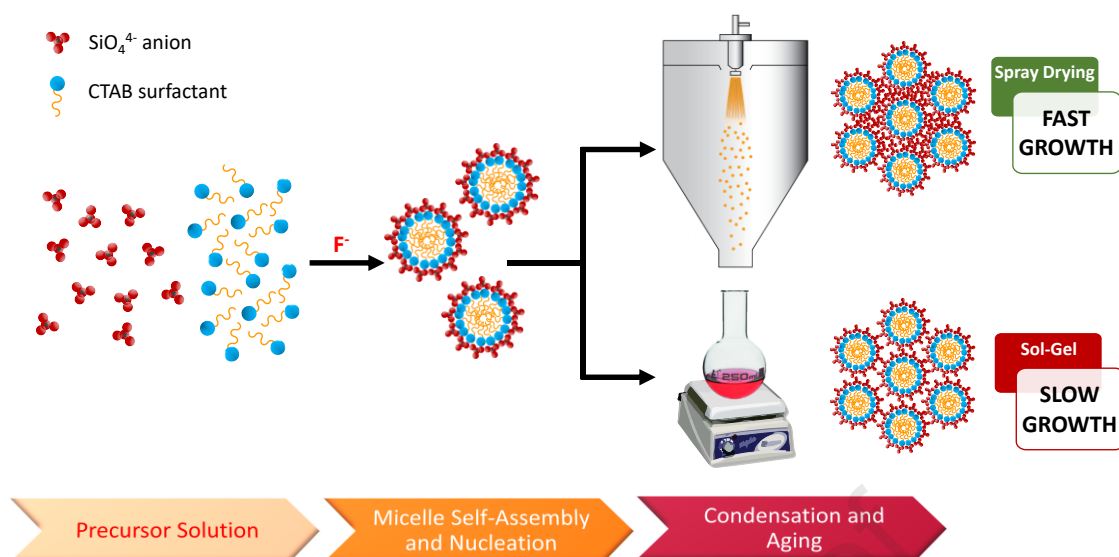


Fig. 6. Artistic representation of the key steps in MSN preparation by the SD method and classical sol-gel synthesis.

However, as seen elsewhere [22,23], fluoride anion is an excellent silica activator even in mild conditions (e.g., neutral pH, room temperature), and it is also able to replace hydroxyl groups from silicate network, reducing the frequency of defects and increasing the stability of the mesoporous structure. Even when the solvent is quickly removed by SD, fluoride is able to catalyze effectively the silicate condensation over CTAB micelles, promoting particle growth and aging in a very short time [23], resulting sample SDN-3 with hexagonal $P6mm$ ordering and good textural properties.

It is remarkable that the observed SDA (cetyltrimethylammonium bromide, CTAB) to silica ratio in the as-synthesized nanoparticles is unusually high ($\text{CTAB}/\text{SiO}_2=0.45$, Table 1) for a mesoporous MCM-41 type material [31]. We think that this is a characteristic of the manufacturing process, that involves the formation of very small droplets (5-6 μm diameter), which are quickly dried by the descendent drying gas stream. Although the droplet remains in suspension enough to allow particle growth, the excess of surfactant accumulates on the external surface.

At this point, gas inlet temperature (T_{in}) becomes crucial to optimize the formation of nanoparticles with the mesoporous structure. For instance, we found that for $T_{in}=90\text{ }^{\circ}\text{C}$ (SDN-3 sample), an optimum assembly between the silicate network building species was achieved during the SD process, with optimum structural and textural properties. Moreover, at $T_{in}=75\text{ }^{\circ}\text{C}$ (SDN-4 sample), although the solvent was fully removed after SD, this material shows lower S_{BET} and V_p values, indicating that a slower evaporation rate may delay and hamper the hexagonal mesophase formation. Conversely, higher gas inlet temperature (e.g., $T_{in}=120\text{ }^{\circ}\text{C}$) provokes very fast solvent evaporation, which affects structure stability and leads to partial pore collapse, minorizing the crystallinity of the sample and its textural properties (SDN-5 sample). In any case, we didn't observe the wet-pocket phenomenon [14], as our nanoparticles were absolutely dried after the SD process, as confirmed by the TGA reports (Fig. S2), and no significant structural changes were found after template removal, as it has been described in other mesoporous materials obtained by SD [32].

We have seen that, even in the best case (sample SDN-3), the observed structural and textural features of the obtained MSNs are far from the unique honeycomb structure of MCM-41, with large surface area, high porosity and narrow mesopore distribution. Indeed, it has been pointed out that the structural array of hexagonally packed pores typical of MCM-41 is hard to be placed in a spherical nanoparticle [33]. Instead, usually MSNs present a broad main peak at low angle (corresponding to the 100 plane), whereas the secondary reflections overlap in a broad band. This happens because the spherical shape of MCM-41 sub-micrometer particles limits the pore ordering in large domains, distorting the hexagonal symmetry and giving rise to broader lines in the XRD pattern [31,33,34]. Accordingly, TEM images of SDN-3 particle revealed a complex pore structure consisting in mainly by wormhole-shaped pores. Really, TEM images only

analyze a very small fraction of the sample, where it is usually difficult to state how much the material is ordered, but the hexagonal symmetry can be found at small domains.

Eventually, it has been shown that the SD process is able to produce well-structured and well-dispersed MSNs by using fluoride as silica mobilizing agent. However, one might question if these nanoparticles are already synthesized in the batch containing the stirring mixture of reagents, so the SD route is only drying quickly already conformed MSNs. To clarify this doubt we carried out the sol-gel synthesis process with the original gel composition at room temperature. We found that, according to ^{29}Si MAS NMR spectra in Fig. 5, the level of connectivity of the silica in the lattice was similar for the sol-gel and SD samples (respectively, SGN-1 and SDN-3). However, powder XRD patterns (Fig. 2) and S_{BET} reports (Fig. 4 and Table 2) made it clear that it was not possible to fully develop the hexagonal ordering by the sol-gel protocol in such a short period ($t=5$ h). Furthermore, the silica and surfactant yields of the sol-gel process were very low ($Y_{\text{SiO}_2}=16\%$, $Y_{\text{CTAB}}=6\%$, Table 1), which is consistent with an uncompleted synthetic procedure, in which most of the silicate and templating molecules are lost in the filtration operation. Therefore, the SD is providing a quick and efficient technique for manufacturing of well-dispersed MSNs with hexagonal $P6mm$ symmetry, and high surface area. Furthermore, this technique is highly scalable and adaptable to the industrial stage.

4. Conclusions

We have shown that it is possible to produce MSNs in a fast and scalable form by SD of the precursor component mixture in fluoride medium and almost neutral pH. The use of fluoride as silica mobilizing agent allows to obtain well-dispersed mesoporous nanoparticles with hexagonal structure in short domains. In addition, it has been shown that the gas inlet temperature (T_{in}) is crucial to optimize the development of the mesoporous structure and, in our case, for $T_{\text{in}}=90$ °C (SDN-3 sample), an optimal

assembly between the silicate network building species was achieved during the SD process, with optimal structural and textural properties.

Declaration of competing interest

The authors declare no competing interest.

Acknowledgements

Financial support by the Spanish National Research Agency [PID2022142952OB-100 grant], Generalitat Valenciana [CIPROM/2021/003 grant] and the Spanish Ministry of Science and Innovation (CEX2021-001230-S grant funded by MCIN/AEI/10.13039/501100011033) is gratefully acknowledged.

Supplementary data

Supplementary Information available: DLS methods and reports. TGA methods and reports.

References

- [1] M. Vallet-Regí, F. Balas, D. Arcos, Mesoporous materials for drug delivery, *Angew. Chem. Int. Ed.* 46 (2007) 7548–7558. <https://doi.org/10.1002/anie.200604488>.
- [2] R.K. Kankala, H. Zhang, C.G. Liu, K.R. Kanubaddi, C.H. Lee, S. Bin Wang, W. Cui, H.A. Santos, K.L. Lin, A.Z. Chen, Metal Species–Encapsulated Mesoporous Silica Nanoparticles: Current Advancements and Latest Breakthroughs, *Adv. Funct. Mater.* 29 (2019). <https://doi.org/10.1002/adfm.201902652>.
- [3] R.K. Kankala, Y.H. Han, J. Na, C.H. Lee, Z. Sun, S. Bin Wang, T. Kimura, Y.S. Ok, Y. Yamauchi, A.Z. Chen, K.C.W. Wu, Nanoarchitected Structure and Surface Biofunctionality of Mesoporous Silica Nanoparticles, *Adv. Mater.* 32 (2020). <https://doi.org/10.1002/adma.201907035>.
- [4] K. Lan, D. Zhao, Functional Ordered Mesoporous Materials: Present and Future, *Nano Lett.* 22 (2022) 3177–3179. <https://doi.org/10.1021/acs.nanolett.2c00902>.

- [5] A. Vely, A. Corma, Advanced zeolite and ordered mesoporous silica-based catalysts for the conversion of CO₂ to chemicals and fuels, *Chem. Soc. Rev.* 52 (2023) 1773–1946. <https://doi.org/10.1039/d2cs00456a>.
- [6] F. Chang, J. Zhou, P. Chen, Y. Chen, H. Jia, S.M.I. Saad, Y. Gao, X. Cao, T. Zheng, Microporous and mesoporous materials for gas storage and separation: A review, *Asia-Pac. J. Chem. Eng.* 8 (2013) 618–626. <https://doi.org/10.1002/apj.1717>.
- [7] K.K. Chenab, B. Sohrabi, A. Jafari, S. Ramakrishna, Water treatment: functional nanomaterials and applications from adsorption to photodegradation, *Mater. Today Chem.* 16 (2020). <https://doi.org/10.1016/j.mtchem.2020.100262>.
- [8] A. Corma, P. Botella, E. Rivero-Buceta, Silica-Based Stimuli-Responsive Systems for Antitumor Drug Delivery and Controlled Release, *Pharmaceutics* 14 (2022). <https://doi.org/10.3390/pharmaceutics14010110>.
- [9] R.K. Kankala, Y.H. Han, H.Y. Xia, S. Bin Wang, A.Z. Chen, Nanoarchitected prototypes of mesoporous silica nanoparticles for innovative biomedical applications, *J. Nanobiotechnology* 20 (2022). <https://doi.org/10.1186/s12951-022-01315-x>.
- [10] P. Botella, I. Abasolo, Y. Fernández, C. Muniesa, S. Miranda, M. Quesada, J. Ruiz, S. Schwartz, A. Corma, Surface-modified silica nanoparticles for tumor-targeted delivery of camptothecin and its biological evaluation, *J. Control. Rel.* 156 (2011) 246–257. <https://doi.org/10.1016/j.jconrel.2011.06.039>.
- [11] F. Gao, P. Botella, A. Corma, J. Blesa, L. Dong, Monodispersed mesoporous silica nanoparticles with very large pores for enhanced adsorption and release of DNA, *J. Phys. Chem. B* 113 (2009) 1796–1804. <https://doi.org/10.1021/jp807956r>.
- [12] V. Candela-Noguera, M. Alfonso, P. Amorós, E. Aznar, M.D. Marcos, R. Martínez-Máñez, In-depth study of factors affecting the formation of MCM-41-type mesoporous silica nanoparticles, *Micropor. Mesopor. Mater.* 363 (2024). <https://doi.org/10.1016/j.micromeso.2023.112840>.
- [13] R.R. Castillo, L. De La Torre, F. García-Ochoa, M. Ladero, M. Vallet-Regí, Production of MCM-41 nanoparticles with control of particle size and structural properties: Optimizing operational conditions during scale-up, *Int. J. Mol. Sci.* 21 (2020) 1–18. <https://doi.org/10.3390/ijms21217899>.
- [14] Z. Yi, L.F. Dumée, C.J. Garvey, C. Feng, F. She, J.E. Rookes, S. Mudie, D.M. Cahill, L. Kong, A New Insight into Growth Mechanism and Kinetics of Mesoporous Silica Nanoparticles by in Situ Small Angle X-ray Scattering, *Langmuir* 31 (2015) 8478–8487. <https://doi.org/10.1021/acs.langmuir.5b01637>.
- [15] K. Okuyama, W.W. Lenggoro, Preparation of nanoparticles via spray route, *Chem. Eng. Sci.* 58 (2003) 537–547. [https://doi.org/10.1016/S0009-2509\(02\)00578-X](https://doi.org/10.1016/S0009-2509(02)00578-X).
- [16] B. Jaime-Escalante, L.M. Melgoza-Contreras, G. Leyva-Gómez, N. Mendoza-Muñoz, Synthesis and drug loading improvements on mesoporous SBA-15 by spray drying, *Drug*

- Dev. Ind. Pharm. 47 (2021) 1895–1903.
<https://doi.org/10.1080/03639045.2022.2075009>.
- [17] A. Ziaee, A.B. Albadarin, L. Padrela, T. Femmer, E. O'Reilly, G. Walker, Spray drying of pharmaceuticals and biopharmaceuticals: Critical parameters and experimental process optimization approaches, *Eur. J. Pharm. Sci.* 127 (2019) 300–318.
<https://doi.org/10.1016/j.ejps.2018.10.026>.
- [18] C. Arpagaus, A Novel Laboratory-Scale Spray Dryer to Produce Nanoparticles, *Dry. Technol.* 30 (2012) 1113–1121. <https://doi.org/10.1080/07373937.2012.686949>.
- [19] K. Waldron, Z. Wu, W.D. Wu, W. Liu, D. Zhao, X.D. Chen, C. Selomulya, Formation of uniform large SBA-15 microspheres via spray drying, *J. Mater. Chem. A* 2 (2014) 19500–19508. <https://doi.org/10.1039/c4ta05002a>.
- [20] M. Varache, I. Bezverkhyy, L. Saviot, F. Bouyer, F. Baras, F. Bouyer, Optimization of MCM-41 type silica nanoparticles for biological applications: Control of size and absence of aggregation and cell cytotoxicity, *J. Non-Cryst. Solids* 408 (2015) 87–97.
<https://doi.org/10.1016/j.jnoncrysol.2014.10.020>.
- [21] A. Corma, M.J. Díaz-Cabañas, M. Moliner, G. Rodríguez, Synthesis of micro- and mesoporous molecular sieves at room temperature and neutral pH catalyzed by functional analogues of silicatein, *Chem. Commun.* (2006) 3137–3139.
<https://doi.org/10.1039/b605909k>.
- [22] F.H.P. Silva, H.O. Pastore, The syntheses of mesoporous molecular sieves in fluoride medium, *Chem. Commun.* (1996) 833. <https://doi.org/10.1039/cc9960000833>.
- [23] W.J. Kim, J.C. Yoo, D.T. Hayhurst, Synthesis of hydrothermally stable MCM-41 with initial adjustment of pH and direct addition of NaF, *Micropor. Mesopor. Mater.* 39 (2000) 177–186. [https://doi.org/10.1016/S1387-1811\(00\)00194-3](https://doi.org/10.1016/S1387-1811(00)00194-3).
- [24] S.J. Milne, H. Mostaghaci, The Influence of Different Drying Conditions on Powder Properties and Processing Characteristics, *Mater. Sci. Eng., A* 130 (1990) 263–271.
[https://doi.org/10.1016/0921-5093\(90\)90067-D](https://doi.org/10.1016/0921-5093(90)90067-D).
- [25] M. Mohammady, Y. mohammadi, G. Yousefi, Freeze-Drying of Pharmaceutical and Nutraceutical Nanoparticles: The Effects of Formulation and Technique Parameters on Nanoparticles Characteristics, *J. Pharm. Sci.* 109 (2020) 3235–3247.
<https://doi.org/10.1016/j.xphs.2020.07.015>.
- [26] M. Kruk, M. Jaroniec, A. Sayari, Application of Large Pore MCM-41 Molecular Sieves To Improve Pore Size Analysis Using Nitrogen Adsorption Measurements, *Langmuir* 13 (1997) 6267–6273. <https://doi.org/https://doi.org/10.1021/la970776m>.
- [27] L. Jin, S.M. Auerbach, P.A. Monson, Simulating the formation of surfactant-templated mesoporous silica materials: A model with both surfactant self-assembly and silica polymerization, *Langmuir* 29 (2013) 766–780. <https://doi.org/10.1021/la304475j>.

- [28] D. Grosso, F. Cagnol, G.J.D.A.A. Soler-Illia, E.L. Crepaldi, H. Amenitsch, A. Brunet-Bruneau, A. Bourgeois, C. Sanchez, Fundamentals of mesostructuring through evaporation-induced self-assembly, *Adv. Funct. Mater.* 14 (2004) 309–322. <https://doi.org/10.1002/adfm.200305036>.
- [29] S.M. Holmes, V.L. Zholobenko, A. Thursøeld, R.J. Plaisted, C.S. Cundya, J. Dwyera, In situ FTIR study of the formation of MCM-41, *J. Chem. Soc., Faraday Trans.* 94 (1998) 2025–2032. <https://doi.org/10.1039/A801898G>.
- [30] I. Indriani, M. Zakir, P. Taba, Samriani, Characterization of mesoporous material MCM-41 after surfactant removal by washing method with HCl-ethanol, in: *AIP Conf. Proc.*, American Institute of Physics, 2024: pp. 0400041–0400045. <https://doi.org/10.1063/5.0222388>.
- [31] P. Botella, A. Corma, M.T. Navarro, Single gold nanoparticles encapsulated in monodispersed regular spheres of mesostructured silica produced by pseudomorphic transformation, *Chem. Mater.* 19 (2007) 1979–1983. <https://doi.org/10.1021/cm0629457>.
- [32] Z. Wu, K. Waldron, X. Zhang, Y. Li, L. Wu, W.D. Wu, X.D. Chen, D. Zhao, C. Selomulya, Spray-drying water-based assembly of hierarchical and ordered mesoporous silica microparticles with enhanced pore accessibility for efficient bio-adsorption, *J. Colloid Interface Sci.* 556 (2019) 529–540. <https://doi.org/10.1016/j.jcis.2019.08.084>.
- [33] B. Pauwels, G. Van Tendeloo, C. Thoelen, W. Van Rhijn, P.A. Jacobs, Structure determination of spherical MCM-41 particles, *Adv. Mater.* 13 (2001) 1317–1320. [https://doi.org/10.1002/1521-4095\(200109\)13:17<1317::AID-ADMA1317>3.0.CO;2-5](https://doi.org/10.1002/1521-4095(200109)13:17<1317::AID-ADMA1317>3.0.CO;2-5).
- [34] S. Schacht, M. Janicke, F. Schü, Modeling X-ray patterns and TEM images of MCM-41, *Micropor. Mesopor. Mater.* 22 (1998) 485–493. [https://doi.org/https://doi.org/10.1016/S1387-1811\(98\)00086-9](https://doi.org/https://doi.org/10.1016/S1387-1811(98)00086-9).



Highlights

1. Spray drying (SD) as an alternative route for the synthesis of mesoporous silica nanoparticles.
2. Optimization of silica mobilizing agent for SD-synthesis of mesoporous silica nanoparticles.
3. Optimization of gas inlet temperature for SD-synthesis of mesoporous silica nanoparticles.

Journal Pre-proof

Declaration of Interests

The authors declare that they have no known competing financial interests or personal relationships that could have appeared to influence the work reported in this paper.

The authors declare the following financial interests/personal relationships which may be considered as potential competing interests:

Pablo Botella reports financial support was provided by Spanish National Research Agency. Pablo Botella reports financial support was provided by Government of Valencia. If there are other authors, they declare that they have no known competing financial interests or personal relationships that could have appeared to influence the work reported in this paper.